Journal of the Optical Society of America A
OPTICS, IMAGE SCIENCE, AND VISION

# Experimental demonstration of ray-rotation sheets

Johannes Courtial,[1,*] Nong Chen,[1] Sean Ogilvie,[1] Blair C. Kirkpatrick,[1] Alasdair C. Hamilton,[1] Graham M. Gibson,[1] Tomáš Tyc,[2] Eric Logean,[3] and Toralf Scharf[3]

[1]School of Physics & Astronomy, College of Science & Engineering, University of Glasgow, Glasgow G12 8QQ, UK
[2]Institute of Theoretical Physics and Astrophysics, Masaryk University, Kotlarska 2, 61137 Brno, Czech Republic
[3]Optics and Photonics Technology Laboratory, Ecole Polytechnique Fédérale de Lausanne, Rue A.-L. Breguet 2, 2000 Neuchâtel, Switzerland
*Corresponding author: johannes.courtial@glasgow.ac.uk

Received 13 March 2018; revised 10 April 2018; accepted 18 April 2018; posted 19 April 2018 (Doc. ID 325977); published 14 June 2018

**We have built microstructured sheets that rotate, on transmission, the direction of light rays by an arbitrary, but fixed, angle around the sheet normal. These ray-rotation sheets comprise two pairs of confocal lenticular arrays. In addition to rotating the direction of transmitted light rays, our sheets also offset ray position sideways on the scale of the diameter of the lenticules. If this ray offset is sufficiently small so that it cannot be resolved, our ray-rotation sheets appear to perform generalized refraction.**



***OCIS codes:*** (080.0080) Geometric optics; (350.3950) Micro-optics.
https://doi.org/10.1364/JOSAA.35.001160

## 1. INTRODUCTION

Generalized refraction can be due to a change of medium at an interface or due to the interface itself, such as in the case of metasurfaces forming thin phase holograms [1]. We consider here the latter case: generalized refraction due to an interface surrounded on both sides with the same homogeneous medium, usually air. In this case, laws of generalized refraction, that is, the relationships between incident and outgoing light-ray directions at the interface, can be divided into those for which a redirected wavefront can be constructed for *any* incident wave, and those for which this is the case only for certain incident waves [2]. In the latter case, the change in light-ray direction introduces, for some incident waves, fractional vortices into the wave, in the worst case at every point on the interface. This implies that such waves are dark everywhere [3], and so the ray-direction change is effectively wave-optically forbidden. All generalized refraction at such optical interfaces to date (e.g., [1,4]) falls into the category which is wave-optically allowed for any incident wave.

This is unfortunate, as the forbidden light-ray-direction changes include gems such as refraction according to a modified Snell's law that leads to perfect ray-optical imaging by planar interfaces [5,6], and rotation of light rays by an arbitrary (but fixed) angle $\alpha$ around the surface normal, which results in objects seen through the device to appear rotated [7], an effect that could perhaps be used as a very compact alternative to existing optical-image-rotation devices (e.g., [8,9]).

But it *is* possible to achieve wave-optically forbidden generalized refraction, at the price of *pixelation*. Pixelated components change the light-ray direction and offset it to a different position on the same pixel. This offset is an unwanted effect, but if the pixels are small, then, from a suitable viewing distance, the pixelation can be as unnoticeable as on a computer monitor's screen. A well-known example of such a pixelated component is the Gabor superlens [10,11], which comprises two parallel microlens arrays with slightly different pitches that are confocal in the simplest case. Pairs of microlenses from the two arrays can be understood as forming miniature telescopes, and the difference in pitch means that the displacement between the optical axes of the two lenses forming a telescope varies across the superlens. These miniature telescopes are the pixels of the device. The Gabor superlens is an example of an integral-imaging device [12,13], a class of optical instruments in which images are formed not by every individual light ray from an object position intersecting the image position (like in stigmatic imaging), but by bundles of light rays—each having passed through a different pixel—intersecting in the image position. Integral imaging is based on, and derives its name from, integral photography [14], which is an early version of light-field photography [15]. The telescopes in a Gabor superlens can perform a number of generalized laws of refraction, including a modified Snell's law [5,16], including negative refraction [17] (but without the perfect imaging [18]), and inversion of one of the ray direction's components ("ray flipping") [19]. A combination

of two ray-flipping sheets can achieve ray rotation around the sheet normal [7,20] and other directions [21]. Only two of these pixelated generalized laws of refraction have so far been demonstrated experimentally, namely ray flipping [22] and modified Snell's-law refraction (e.g., [6,11,23]).

Here we demonstrate experimentally sheets that perform local light-ray rotation. The sheets are designed such that the rotation is around a local axis perpendicular to the sheet. The resulting view of a plane parallel to the sheet is rotated and magnified. We measure the rotation angles and confirm that they agree with theory. In the form of (undesired) "ghost images," we also unwittingly demonstrate light-ray rotation around directions other than the local sheet normal.

## 2. EXPERIMENT

Our ray-rotating sheets are pairs of ray-flipping sheets in parallel, and nearby, planes. Each ray-flipping sheet, in turn, consists of a pair of lenticular arrays, positioned such that their focal planes coincide (Fig. 1). The experiment simply consists of taking photos through different ray-rotating sheets.

We had previously built ray-flipping sheets experimentally [22], but combining these into ray-rotating sheets was more difficult than we had anticipated: two of the sheets described in [22], combined into ray-rotating sheets, are almost opaque (too many optical surfaces); work well enough only in a tiny fraction of the sheet area (the lenticular arrays are not sufficiently flat for their focal planes to coincide across the entire sheet area); and do not produce the correct angle by which objects appear rotated when seen through the ray-rotating sheet (because the cylindrical lenslets in the two lenticular arrays that formed each ray-flipping sheet were not sufficiently parallel).

Our new ray-flipping sheets consist of various commercial lenticular arrays [the experiments described here were performed with Lenstar 50 LPI (lenticules per inch) arrays], normally used for applications such as 3D postcards. These lenticular arrays are manufactured with a planar surface in the cylindrical lenslets' focal plane; the cylindrical lenslets are formed by bumps on the other surface. We used UV-curing glue to attach the planar surfaces of two lenticular arrays to each other, after careful manual alignment that seeks to make the cylindrical lenslets in the two arrays parallel, and to minimize their offset. The careful alignment is not sufficiently consistent to produce, every time, ray-flipping sheets of sufficient quality, so we produced many (≈30) sheets and used the best. The glue drastically improves the transparency of the sheets, and the glued sheets are very easy to handle. Altogether, the quality of the sheets is sufficient for our purposes.

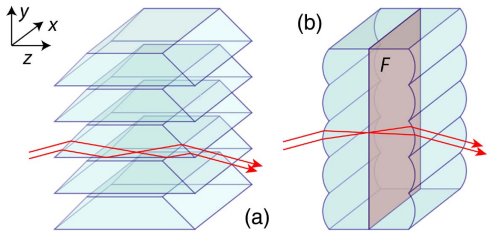


**Fig. 1.** Possible realizations of ray-flipping sheets. (a) Ray-flipping sheets were initially proposed in the form of an array of Dove prisms [19]. (b) The first experimental demonstration [22] used confocal lenticular arrays ($F$ is the common focal plane).

Figure 2 shows photos of a Rubik's cube taken through various ray-rotating sheets created simply by holding two ray-flipping sheets. Obvious imperfections, in the form of spatially dependent blurring, ghost images, and unwanted light scattering, are clearly visible. The ray-rotation angles were ≈0°, for which the cube is almost undistorted; ≈90°, which is an example of a sheet which—in its idealized form—is wave-optically forbidden [3]; and ≈180°, which is the situation described in [17], and which corresponds to negative refraction with a refractive index ratio $n_1/n_2 = -1$ and produces an image of the cube that is pseudoscopic, i.e., the back of the cube appears closer than the front (which is why it also appears bigger). Note that, in the image that corresponds to a ray-rotation angle of ≈90°, different parts of the cube that are at different distances from the sheet appear rotated by different angles, as predicted by the equation for the apparent rotation angle which we derive below [Eq. (4)]. Note also that our ray-rotating sheets are different from the moiré magnifier [23], which also appears to rotate objects viewed through it: the former is homogeneous in the sense that the law of refraction is the same at each position; the latter changes light-ray direction differently at different positions.

It is perhaps worth mentioning, without proof other than the diagrams shown in Fig. 3, that it can be shown that confocal lenticular arrays in which the cylindrical lenses are parallel to, but also displaced relative to, those of the other array [Fig. 3(b)]

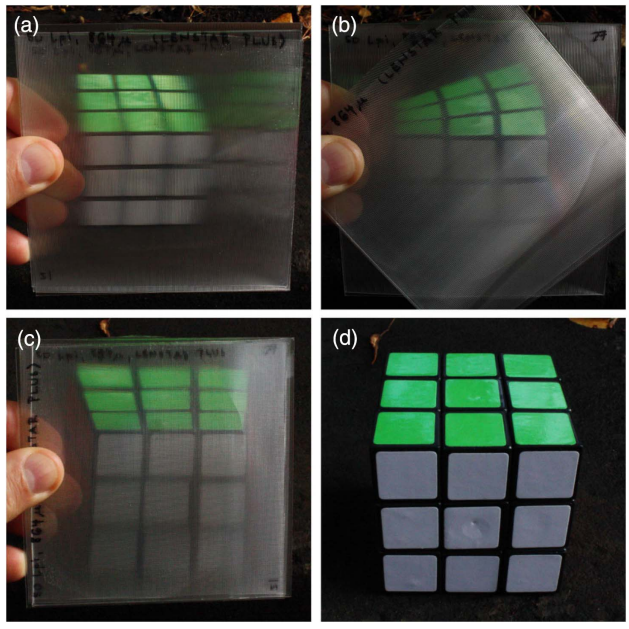


**Fig. 2.** Views through different ray-rotating sheets. The ray-rotation angles are (a) ≈0° (parallel ray-flipping sheets); (b) ≈90° (actually 82°; the ray-flipping sheets are rotated through 41°); (c) ≈180° (ray-flipping sheets rotated through 90°). Clearly visible imperfections include blurring and additional images [visible in (a); an additional image can be seen to the right of the main image] and light scattering [resulting in a milky appearance of the sheets, clearly visible in (b) and (c)]. The object seen through the sheets, a Rubik's cube, is shown without a sheet in (d). Rubik's Cube® used with permission from Rubik's Brand Ltd.

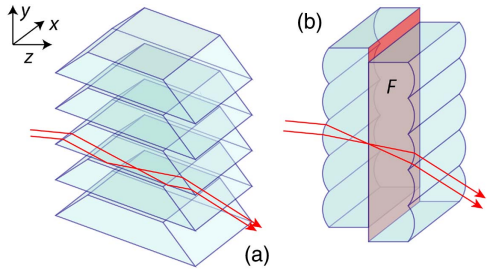


**Fig. 3.** (a) Array of inclined Dove prisms and (b) displaced confocal lenticular arrays.

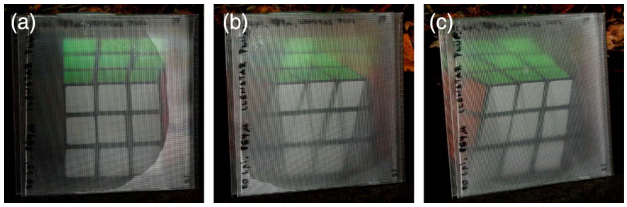


**Fig. 4.** View through a ray-rotating sheet ($\alpha \approx 180°$) from different directions. (a) was taken from a position approximately head-on. It shows the main image. (b) and (c) were taken from positions further and further to one side. In (b) a ghost image becomes visible; in (c) the main image has disappeared almost completely. Rubik's Cube® used with permission from Rubik's Brand Ltd.

redirect light rays that are incident from a range of directions like arrays of inclined Dove prisms [Fig. 3(a)]. The same can be true in non-displaced lenticular arrays, namely for light rays undergoing non-standard refraction, i.e., light rays that pass through non-corresponding (i.e., not directly opposite) cylindrical lenslets, which give rise to additional "ghost" images [24,25]: clearly this is equivalent to a displacement that equals the separation between neighboring lenses. A combination of two such arrays is then a sheet that rotates light-ray direction by an arbitrary (but fixed) angle around a local axis other than the sheet normal [21].

Figure 4 shows the view through a ray-rotating sheet from directions that are different enough for ghost images to become visible. We have therefore also demonstrated local light-ray rotation around an axis other than the sheet normal.

## 3. MEASUREMENT OF APPARENT ROTATION ANGLE

Our sheets allow us to measure the angle by which planar objects parallel to the ray-rotating sheet appear rotated when seen through the sheet. This apparent rotation is somewhat counterintuitive: extended objects appear not simply rotated by the ray-rotation angle, but they can appear twisted [see Fig. 2(b)]. The reason is that the angle by which an object appears rotated depends on the ratio of the distance $z_1$ between the object and the ray-rotation sheet and the distance $z_2$ between the ray-rotation sheet and the observer. It can be calculated by considering a bundle of light rays originating from a point light source L, passing through a ray-rotation sheet, and eventually hitting the position of an observer's eye, E [Fig. 5(a)]. The observer only sees L if any light ray from L actually reaches E; L then appears to be in the direction from which those light rays approach E.

We assume that one such light ray exists and calculate the position P on the ray-rotation sheet through which it passes. We consider the orthographic projection of L and E into the plane of the ray-rotation sheet (of course, P is already in this plane), and identify this plane with an Argand plane whose origin coincides with the projection of E. We then describe the projections of L, P, and E by complex numbers $L$, $P$, and $E = 0$; we also define $p_1 = P - L$ (which is the projection of the light ray from L to P) and $p_2 = E - P$ (the projection of the light ray from P to E). This is shown in Fig. 5(b).

We now use the fact that the ray-rotation sheet rotates the ray direction around the sheet normal, which means that the angles with the sheet normal of the rays in front of and behind the ray-rotation sheet are the same. This means that the tangents of these angles are also the same, and so $|p_1|/z_1 = |p_2|/z_2$. We also note that the angle between the $p_1$ and $p_2$ is the angle $\alpha$ by which the ray-rotation sheet rotates the light-ray direction around the sheet normal, and so

$$p_2 = p_1 \frac{z_2}{z_1} \exp(i\alpha). \tag{1}$$

Solving this equation, together with the equations $L + p_1 = P$ and $P + p_2 = E = 0$, for $P$ yields

$$P = \frac{L}{1 + (z_1/z_2)\exp(-i\alpha)}. \tag{2}$$

Note that this solution for $P$ is unique and always exists, which confirms our earlier assumption.

In the absence of the sheet, the observer would see L in the direction of a position in the plane of the ray-rotation sheet that corresponds to the complex number

$$P_0 = P(\alpha = 0) = L\frac{z_2}{z_1 + z_2}. \tag{3}$$

Compared to the absence of the sheet, when seen through the ray-rotation sheet L therefore appears to come from a position in the plane of the sheet that is rotated by an angle

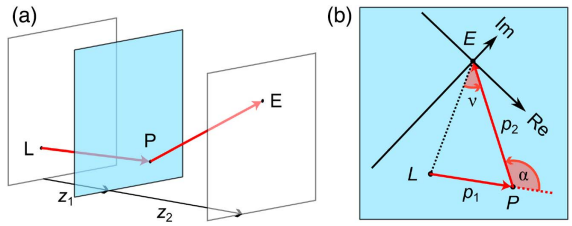


**Fig. 5.** Calculation of the angle, $\nu$, by which a point light source, L, appears rotated when it is seen through a ray-rotating sheet from eye position E. (a) Three-dimensional positions of the light source and observer relative to the ray-rotating sheet. The sheet is in the shaded plane; P is the point where the light ray from L the observer sees passes through the sheet. (b) Orthographic projection into the plane of the ray-rotation sheet, into which an Argand plane has been placed whose origin coincides with the projection of E. $L$, $P$, and $E = 0$ are the complex numbers that correspond to the orthographic projections of L, P, and E. [Adapted from [7], Figs. 5(a) and 5(b). ]

$$\nu = \arg\frac{P}{P_0} = \tan^{-1}\left(\frac{\sin\alpha}{z_2/z_1 + \cos\alpha}\right) \quad (4)$$

around the orthographic projection of E (note that, in [7], a similar—but not identical—approach was used to calculate the angle $\nu$, but the result, Eq. (8) in [7], was wrong) and whose distance from the orthographic projection of E is stretched by a factor

$$\left|\frac{P}{P_0}\right| = \left|\frac{1 + z_2/z_1}{1 + \exp(i\alpha)z_2/z_1}\right|. \quad (5)$$

As, for a fixed ray-rotation angle $\alpha$ and observer position, this rotation angle and stretch factor depends only on the ratio of $z_1$ and $z_2$, entire extended objects in planes parallel to the ray-rotation sheet are rotated and stretched in this way. That the rotation angle depends on the distances explains the counterintuitive twisting of extended objects.

For the measurement of the apparent rotation angle, we used a digital single-lens reflex camera (Canon EOS 450D with Canon EF 100 mm $f/2.8$ Macro USM lens). The camera distance is the distance between the sheet and the lens's entrance pupil, the position of which we determine using parallax. The position of the entrance pupil changes with focusing distance; to facilitate the analysis, we use our lens with the same focusing distance (1 m) throughout the experiment. Note that the ray-rotating sheet does not produce geometrical images of the object anyway (unless the ray-rotation angle is either 0° or 180° [7]), so the focusing distance is not as important as it normally is. In order to see sharp images, we use the lens with its smallest aperture opening, $f/32$.

With a fixed camera distance, $z_2$, we took photos of a grid pattern (insets in Fig. 6) various distances $z_1$ behind the sheet. We determined the angle between the two constituent ray-flipping sheets from the photos (using Adobe Illustrator), in which the individual lenses are visible (note that aliasing effects in the pattern of the cylindrical lenses of the array that is seen through the other array of lenses can lead to the wrong angle being picked); the ray-rotation angle $\alpha$ is twice that angle. From the photos we determined (again using Adobe Illustrator) the angle by which the vertical grid lines close to the center, when seen through the ray-rotating sheet, were rotated with respect to the same lines seen with the sheet removed. The graph in Fig. 6 shows a comparison of the predicted and measured apparent rotation angles. Note that there are no free parameters, and note the excellent agreement between theory and experiment. We repeated this procedure for other ray-rotation angles, in each case reaching excellent agreement.

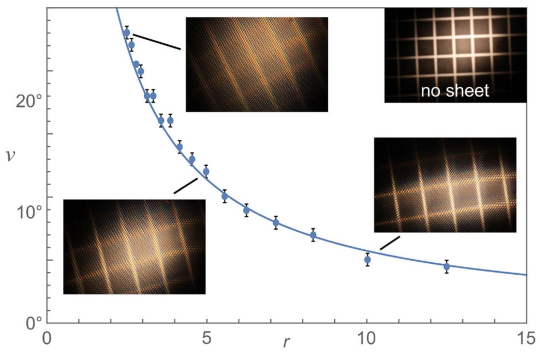


**Fig. 6.** Apparent rotation angle of a planar object when seen through a sheet that rotates light-ray rotation through $\alpha = 92°$ around the local sheet normal for different values of $r$. Points mark measurements, and the solid line was calculated according to Eq. (4). Insets show photos of the test pattern seen on its own ("no sheet") and through the ray-rotating sheet for different values of $z_1$. In all cases, $z_2 = 50$ cm. Visible imperfections include blurring and view distortion, leading to a different apparent rotation angle at different points in the photo (the error bars, which correspond to ±0.5°, indicate the estimated average effect these imperfections have on the measured values).

In the photos shown in Fig. 6, imperfections are clearly visible. These include some blurring and a slight distortion. The constancy throughout the experiment of the focusing distance (for reasons explained above) certainly contributes to the blurring, and a slight lack of flatness of the lenticular arrays contributes to the distortion. Perhaps more importantly, we believe that all of the imperfections are at least partly due to slight misalignment: the blurring is partly due to a slight error in the separation of the two lenticular arrays that make up each ray-flipping sheet (so they are not exactly confocal); and the distortion is due to a slight variation in alignment across the sheets. All of these could be fixed by extruding each ray-flipping sheet as one element, rather than two elements that subsequently have to be aligned and glued together.

## 4. CONCLUSIONS

We have shown here that ray-rotating sheets can be realized experimentally. Imperfections in the sheets are clearly visible. Utilizing advances made in the context of imaging devices that use lenslet arrays or lenticular arrays (e.g., [26]), we are currently working on improving the optical quality of our components and on developing applications.

**Funding.** Engineering and Physical Sciences Research Council (EPSRC) (EP/M010724/1); Grantová Agentura České Republiky (GACR) (P201/12/G028).

## REFERENCES

1. N. Yu, P. Genevet, M. A. Kats, F. Aieta, J.-P. Tetienne, F. Capasso, and Z. Gaburro, "Light propagation with phase discontinuities: generalized laws of reflection and refraction," Science **334**, 333–337 (2011).
2. J. Courtial and T. Tyc, "Generalised laws of refraction that can lead to wave-optically forbidden light-ray fields," J. Opt. Soc. Am. A **29**, 1407–1411 (2012).
3. A. C. Hamilton and J. Courtial, "Metamaterials for light rays: ray optics without wave-optical analog in the ray-optics limit," New J. Phys. **11**, 013042 (2009).
4. F. Aieta, P. Genevet, N. Yu, M. A. Kats, Z. Gaburro, and F. Capasso, "Out-of-plane reflection and refraction of light by anisotropic optical antenna metasurfaces with phase discontinuities," Nano Lett. **12**, 1702–1706 (2012).
5. J. Courtial, "Ray-optical refraction with confocal lenslet arrays," New J. Phys. **10**, 083033 (2008).
6. J. Courtial, B. C. Kirkpatrick, E. Logean, and T. Scharf, "Experimental demonstration of ray-optical refraction with confocal lenslet arrays," Opt. Lett. **35**, 4060–4062 (2010).
7. A. C. Hamilton, B. Sundar, J. Nelson, and J. Courtial, "Local light-ray rotation," J. Opt. A **11**, 085705 (2009).

8. E. G. Paek, J. Y. Choe, T. K. Oh, J. H. Hong, and T. Y. Chang, "Nonmechanical image rotation with an acousto-optic dove prism," Opt. Lett. **22**, 1195–1197 (1997).
9. Y. Yan, "Optical image rotating device used with afocal image relaying optics and laser diode array," U.S. patent 6,243,210 (June 5, 2001).
10. D. Gabor, "Improvements in or relating to optical systems composed of lenticules," UK patent 541,753 (December 10, 1941).
11. C. Hembd-Sölner, R. F. Stevens, and M. C. Hutley, "Imaging properties of the Gabor superlens," J. Opt. A **1**, 94–102 (1999).
12. R. F. Stevens and T. G. Harvey, "Lens arrays for a three-dimensional imaging system," J. Opt. A **4**, S17–S21 (2002).
13. X. Xiao, B. Javidi, M. Martinez-Corral, and A. Stern, "Advances in three-dimensional integral imaging: sensing, display, and applications invited," Appl. Opt. **52**, 546–560 (2013).
14. G. Lippmann, "La photographie intégrale," Comptes Rendus Acad. Sci. **146**, 446–451 (1908).
15. R. Ng, M. Levoy, M. Brédif, G. Duval, M. Horowitz, and P. Hanrahan, "Light field photography with a hand-held plenoptic camera," Tech. Rep. CTSR 2005-02 (Stanford University, 2005).
16. A. C. Hamilton and J. Courtial, "Generalized refraction using lenslet arrays," J. Opt. A **11**, 065502 (2009).
17. J. Courtial and J. Nelson, "Ray-optical negative refraction and pseudoscopic imaging with Dove-prism arrays," New J. Phys. **10**, 023028 (2008).
18. J. B. Pendry, "Negative refraction makes a perfect lens," Phys. Rev. Lett. **85**, 3966–3969 (2000).
19. A. C. Hamilton and J. Courtial, "Optical properties of a Dove-prism sheet," J. Opt. A **10**, 125302 (2008).
20. B. Sundar, A. C. Hamilton, and J. Courtial, "Fermat's principle and the formal equivalence of local light-ray rotation and refraction at the interface between homogeneous media with a complex refractive index ratio," Opt. Lett. **34**, 374–376 (2009).
21. A. C. Hamilton, B. Sundar, and J. Courtial, "Local light-ray rotation around arbitrary axes," J. Opt. **12**, 095101 (2010).
22. M. Blair, L. Clark, E. A. Houston, G. Smith, J. Leach, A. C. Hamilton, and J. Courtial, "Experimental demonstration of a light-ray-direction-flipping METATOY based on confocal lenticular arrays," Opt. Commun. **282**, 4299–4302 (2009).
23. M. C. Hutley, R. Hunt, R. F. Stevens, and P. Savander, "The moiré magnifier," Pure Appl. Opt. **3**, 133–142 (1994).
24. J. Courtial, "Standard and non-standard metarefraction with confocal lenslet arrays," Opt. Commun. **282**, 2634–2641 (2009).
25. T. Maceina, G. Juzeliūnas, and J. Courtial, "Quantifying metarefraction with confocal lenslet arrays," Opt. Commun. **284**, 5008–5019 (2011).
26. M.-S. Kim, T. Scharf, S. Mühlig, M. Fruhnert, C. Rockstuhl, R. Bitterli, W. Noell, R. Voelkel, and H. P. Herzig, "Refraction limit of miniaturized optical systems: a ball-lens example," Opt. Express **24**, 6996–7005 (2016).